Supplementary Information

Materials and Methods

All animal experiments were approved by the Thüringer Landesamt für Lebensmittelsicherheit und Verbraucherschutz (TLLV) in Germany.

Generation of Ae1^{R607H} knock-in mice

A clone isolated from a 129/SvJ mouse genomic λ library (Stratagene, now Agilent, Santa Clara, CA, USA) was used to construct the targeting vector. A ~13.25 kb fragment including exons 2-18 of the *Ae1* gene was cloned into the pKO-V901 plasmid (Lexicon Genetics, The Woodlands, TX, USA) with a phosphoglycerate kinase (pgk) promoter-driven diphtheria toxin A cassette. A pgk promoter-driven neomycin resistance cassette flanked by loxP sites was inserted into the *Pci*I site of intron 9. The R607H point mutation was introduced by site-directed mutagenesis into a subcloned *Bst*Z17I-*Spe*I fragment (1541 bp) harboring exon 14. The construct was linearized with *Not*I and electroporated into R1 mouse embryonic stem (ES) cells. Neomycin-resistant clones were analyzed by Southern blot using *Hind*III and an external probe of 779 bp (Chromosome 11, 102350002-102350780) was amplified with primers "Ae1_SB1_for" (5'-GTC TAT ATG CAG GCC TTT GTC-3') and "Ae1_SB1_rev" (5'-CAT GAA AAG TGT CCT CCG T-3'). Two correctly targeted ES cell clones were injected into C57BL/6 blastocysts to generate chimeras. Chimeric mice were mated to a cre-Deleter mouse strain to remove the selection cassette (1). Studies were performed in a mixed 129Sv/C57BL/6 background in the F4 and F5 generation. Genotypes were determined by PCR of tail biopsy DNA. For PCR genotyping, the forward primer F1 (5′-TAG CTC CTT CTA CCC CAC CCA-3′) and the reverse primer R1 (5′-CCA GAG GTA CAT GGT AAA ACA TTG TC-3′) were used in a single PCR mix allowing detection of the 189 bp wild-type allele and the 320 bp knock-in (KI) allele. Detection of the introduced point mutation was performed by Sanger sequencing of the 498 bp PCR product amplified by forward primer F1 (5′-GCT CAA GTC AAG GCT TGG ATG G-3′) and reverse primer R1 (5′- CAA GGA TTC TGC TCA TCC GGA-3′).

NH_4Cl loading

We initially planned to study 8 mice from each genotype. However, as insufficient numbers of wild-type mice were available at the time metabolic cage experiments began, we increased the number of heterozygous mice. Thus, n=6 *Slc4a1*$^{+/+}$; n=10 *Slc4a1*$^{R607H/+}$; n=8 *Slc4a1*$^{R607H/R607H}$ 3-month-old male littermates were housed in metabolic cages with one mouse per cage (Tecniplast, Buguggiate, Italy). Urine was collected daily under mineral oil. After adaptation to metabolic cages and recording of baseline parameters drinking water was supplemented with 0.28 M NH_4Cl for 6 days. The pH of urine samples was measured with a pH microelectrode (InLab Micro pH, Mettler Toledo, Viroflay, France) and samples were immediately frozen before further analysis. Retro-orbital blood was collected at days 3 and 6 following acid loading and analyzed with an ABL 77 pH/blood-gas analyser (Radiometer, Copenhagen, Denmark). Urinary ammonium and titratable acid were measured by titration with a DL 55 titrator (Mettler Toledo, Viroflay, France). Urine osmolalities were determined by freezing point osmometer (Roebling, Berlin, Germany). Urine creatinine was measured by Jaffé colorimetric method. Urinary Na^+ and K^+ were measured by flame photometry (IL 943; Global Medical Instrumentation, Ramsey, MN, USA). Urine aldosterone was measured via RIA (DPC Dade Behring, now Siemens Healthcare, Erlangen, Germany).

Histology and immunohistochemistry

Kidneys were fixed by retrograde perfusion of the aorta with 4 % PFA in phosphate buffer. Dissected kidneys were washed in ice-cold phosphate-buffered saline (PBS) for 30 minutes and flash frozen in isopentane cooled with liquid nitrogen. 6 µm thick cryosections were subjected to Masson-Goldner stain or von Kossa stain. Kidney sections from a4 knockout mice served as a positive control (2). For immunohistochemistry, cryosections were blocked with goat or donkey serum (3). Sections were incubated overnight at 4°C with primary antibody, washed with PBS, incubated with fluorophore-conjugated secondary antibody, washed with PBS and then mounted with Glycergel mounting medium (DAKO/Agilent, Santa Clara, CA, USA). Each experiment included three mice per group. Representative images were acquired with a Confocal SP8 workstation (Leica, Wetzlar, Germany).

Cell culture

M1 (cortical collecting duct cells, ATCC CRL-2038) and mIMCD-3 cells (ATCC CRL-2123) underwent infection with Mouse moloney leukemia virus to induce quasi-stable expression of human kidney anion exchanger 1 (kAE1) WT-myc, of R589H-HA (the human equivalent of R607H), or of both kAE1 WT-myc and kAE1 R589H-HA, as previously described (4). However, despite continued G418 exposure of cell cultures (1 mg/ml for M1 cells; 2 mg/ml for mIMCD-3 cells), kAE1 protein expression declined over a two-to-three week period. For immunostaining, cells were grown for 7 days on semi-permeable filter supports, fixed with 4 % paraformaldehyde, quenched, rinsed, and permeabilized with 0.1 % Triton X-100, and blocked with 1 % bovine serum albumin in PBS. Epitope-tagged kAE1 proteins were detected either with mouse anti-myc (Cell Signalling, Danvers, MA, USA) or mouse anti-HA antibodies (Covance, Princeton, NJ, USA), each followed by Cy3-coupled anti-mouse Ig (Jackson ImmunoResearch laboratories, West Grove, PA, USA). Samples were examined with an IX81 microscope (Olympus, Tokyo, Japan) equipped with a Nipkow spinning-disk (Quorum Technologies, Guelph, Canada).

Counting of intercalated cells

Kidney sections were co-stained either for AE1, pendrin, and V-type ATPase E subunit (Atp6v1e1) or for AE1, pendrin, and AQP2. Ten random fields from cortex and inner stripe of the outer medulla (ISOM) were acquired at 20X magnification. Numbers of type A intercalated cells (basolateral AE1 expression), and type B intercalated cells (apical pendrin expression) were counted (n=3 mice per genotype). The experimenter was blinded for the genotype.

Electron microscopy

After perfusion *in situ* with 4 % PFA as above, tissues were shipped in fixative to Boston, and further fixed in 2 % glutaraldehyde in 0.1 M sodium cacodylate pH 7.4 (Electron Microscopy Sciences, Hatfield, PA, USA). Tissues were then rinsed in cacodylate buffer and post-fixed in 1 % osmium tetroxide (Electron Microscopy Sciences) in 0.1 M cacodylate buffer for 1 h at room temperature, and rinsed as above. Specimens were dehydrated briefly in 100% propylene oxide, and infiltrated in a 1:1 solution of EPON (Ted Pella Inc., Redding, CA, USA) and 100 % propylene

oxide overnight. Specimens were allowed to infiltrate in fresh 100% EPON for several hours, embedded in 100% EPON, and allowed to polymerize overnight in a 60°C oven. Ultrathin sections were cut on a Leica EMUC7 ultramicrotome (Leica Microsystems, Buffalo Grove, IL, USA), collected on formvar-coated grids, stained with lead citrate and uranyl acetate, and examined at 80 kV in a JEOL 1011 transmission electron microscope (TEM; JEOL, Peabody, MA, USA). Images were acquired using an AMT digital imaging system (Advanced Microscopy Techniques, Danvers, MA, USA).

For immunogold staining, samples fixed in 4 % paraformaldehyde alone were embedded in LRWhite resin as previously described (5). Ultrathin sections were incubated for 2 h with anti-AE1 or V-type ATPase antibodies, rinsed, incubated for 45 min with gold-labeled goat anti-guinea-pig or goat anti-rabbit Ig (Ted Pella), and counterstained with uranyl acetate before imaging as above with the JEOL 1011 TEM.

Immunoblotting

Mice were perfused transcardially with PBS at room temperature (RT). Perfused kidneys were placed in ice-cold PBS and homogenized in ice-cold isolation buffer (250 mM sucrose, 20 mM Tris-Hepes, pH 7.4) supplemented with protease inhibitor cocktail (Complete; Roche Diagnostics, Risch-Rotkreuz, Switzerland) and phosphatase inhibitor cocktail (PhosSTOP; Roche Diagnostics). Cellular debris was removed by centrifugation at 4,000 g for 15 min at 4°C. Membrane-enriched fractions were prepared by centrifugation at 17,000 g for 30 min at 4°C. Protein concentration was determined using the Bradford protein assay (microBradford, BioRad, Hercules, CA, USA). Total homogenates and membrane-enriched fractions were prepared with 6x SDS-loading buffer (0.375 mM Tris-HCl pH 6.8, 12 % SDS, 0.6 M dithiothreitol, 60 % glycerol and bromophenol blue) and incubated for 30 min at room temperature. 15-30 µg of protein were loaded on 10 % polyacrylamide gels (XCell *SureLock* Mini-cell; Invitrogen Life Technologies, Carlsbad, CA, USA) separated and blotted onto a nitrocellulose membrane. Membranes were blocked with 5 % milk in Tris-buffered saline (TBS) and incubated overnight at 4°C with the primary antibody. The secondary horseradish-conjugated anti-Ig antibody was incubated on membranes for 2 h at RT, detected with Pierce ECL Western Blotting Substrate (Thermo Scientific,

Waltham, MA, USA), and analyzed by LAS 4000 ImageQuant (GE Healthcare, Little Chalfont, UK).

Half-life measurement

M1 or mIMCD-3 cells expressing kAE1 WT-myc or kAE1 R589H-HA were plated to sub-confluency on 6-well plates, then incubated for 0, 4, 8, 16 or 24 h with 10 µg/ml cycloheximide in DMEM:F12 culture medium supplemented with 10 % fetal bovine serum and 1 mg/ml penicillin/streptomycin. Cells were lysed in PBS containing 1 % Triton X-100, 1 µg/ml aprotinin, 2 µg/ml leupeptin, 1 µg/ml pepstatin A, and 100 µg/ml PMSF. kAE1 polypeptides were subjected to immunoblot analysis using mouse anti-HA or anti-myc antibody, followed by horseradish peroxidase-coupled anti-mouse Ig (Cell Signaling, Danvers, MA, USA). Bound peroxidase was detected by enhanced chemiluminescence (ECL Prime; GE Healthcare) and relative band intensities were analyzed with ImageJ (National Institutes of Health, Bethesda, MD, USA).

AE1-mediated transport activity in red blood cells by stopped-flow analysis

200 µl mouse blood was washed three times in PBS. Washed red blood cells were resuspended in 32 ml hypotonic lysis buffer (7 mM KCl, 10 mM Hepes/KOH, pH 7.2) for 40 min on ice, followed by resealing for 1h at 37°C in resealing buffer (100 mM KCl, 10 mM Hepes/KOH, pH 7.2, 1 mM $MgCl_2$ and 2 mg/ml bovine carbonic anhydrase) containing 0.15 mM of the fluorescent pH sensitive dye pyranine (1-hydroxypyrene-3,6,8-trisulfonic acid, Sigma-Aldrich, St. Louis, MO, USA). After three washes in ice-cold incubation buffer (100 mM KCl, 10 mM Hepes/KOH, pH 7.2), resealed ghosts were kept on ice until stopped-flow experiments were performed (6) at 30°C (SFM400; Bio-logic, Grenoble, France). Excitation was at 465 nm and emitted light was filtered with a 520 nm cut-off filter. For measurement of HCO_3^-/Cl^- exchange activity, dye-loaded ghosts resuspended in 3 ml “chloride buffer” (100 mM KCl and 10 mM HEPES/KOH pH 7.2) were rapidly mixed with an equal volume of bicarbonate buffer (100 mM $KHCO_3$ and 10 mM HEPES/HCl pH 7.2), generating an inwardly directed HCO_3^-/CO_2 gradient of 50 mEq/L and an outwardly directed Cl^- gradient of equal magnitude. Data from six-to-eight time courses were averaged and fit to a mono-exponential function using the simplex procedure of Biokine software (Bio-logic).

Surface AE1 expression on erythrocytes was determined by immunostaining with an anti-Diego b (Dib) antibody followed by flow cytometric analysis on a FACSCanto II flow cytometer (Becton-Dickinson, Franklin Lakes, NJ, USA). Secondary antibodies were goat anti-human PE-conjugated F(ab')2 fragments (Beckman Coulter, Brea, CA, USA). Results were analysed using FlowJo software (FlowJo, Ashland, OR, USA).

AE1 transport in mIMCD-3 cells

mIMCD-3 cells expressing either kAE1 WT, R589H, or WT and R589H mutant were grown on glass coverslips to 70 % confluence. AE1 transport activity was measured using BCECF-AM (Sigma-Aldrich) as described previously (7). After washing with serum-free OptiMEM medium (Gibco/ Thermo Fisher), coverslips were incubated with 10 µM BCECF-AM (Sigma-Aldrich) for 10 min at 37°C. Coverslips were then placed in fluorescence cuvettes and the cells were perfused at room temperature with: 5 mM glucose, 5 mM K^+ gluconate, 1 mM Ca^{2+} gluconate, 1 mM $MgSO_4$, 10 mM Hepes, 2.5 mM NaH_2PO_4, 25 mM $NaHCO_3$, 140 mM chloride, followed by a chloride-free medium containing 140 mM gluconate to induce intracellular alkalization. Solutions were continuously bubbled with 5 % CO_2. Using a PTI fluorimeter (Photon Technologies International (PTI), Edison, NJ, USA), fluorescence was excited at 440 and 490 nm, and fluorescence emission was recorded at 510 nm. Intracellular BCECF fluorescence was calibrated with buffers at pH values of 6.5, 7.0, or 7.5, each containing 100 µM nigericin sodium salt. Cellular anion exchange rates were determined by linear regression of the initial 60 s of fluorescence perturbation, and normalized to pH calibration measurements, using FelixGX 4.1.0 software (PTI). Results represent $\geq$ 3 independent experiments.

Reverse transcription and quantitative PCR

Total RNA (2 µg from renal cortex or medulla; 5 µg from liver) was reverse-transcribed with SuperScript III Reverse Transcriptase (Invitrogen Life Technologies, Carlsbad, CA, USA) as described previously (8). Duplicate qPCR reactions were perfomed with SsoFast EvaGreen Supermix (BioRad, Hercules, CA, USA) using a CFX96 Touch Real-Time PCR Cycler (BioRad). Primer sequences were "flAe1_for" (5'-CCCCATACACCATCCTCTC-3' and "flAe1_rev" (5'-CGGTTATGCGCCATGGA-

3'), and we used the ActB Quantitect Primer Assay QT01136772 (Qiagen, Hilden, Germany).

Antibodies

Primary antibodies use in this study were: rabbit anti-NBCn1 (9) (Western Blot 1:5000; Immunofluorescence 1:2500); rabbit anti-rkNBC1 (10) (WB 1:5000); rabbit anti-NHE3 (Catalog number SPC-400, StressMarq Biosciences, Victoria, BC, Canada); rabbit anti-AE2 (11); rabbit anti-pendrin (12) (WB 1:10000); rabbit anti-V-type ATPase B1 subunit (Atp6v1b1) (13) (WB 1:30,000); chicken anti-Atp6v1e1 subunit (14) (IF 1:500); guinea pig anti-AE1 (15) (IF 1:5000); guinea pig anti-pendrin (15) (IF 1:1000); mouse anti-p62 (anti-SQSTM1, ab56416, Abcam, Cambridge, UK); rabbit anti-Ubiquitin (DAKO/Agilent), goat anti-AQP2 (C-17; Santa Cruz, Dallas, TX, USA) (IF 1:1000); anti-Diego b (1:4) human monoclonal antibodies were kindly donated by Dr. M. Uchikawa, Japanese Red Cross Central Blood Center, Tokyo, Japan; mouse anti-HA (Covance, Princeton, NJ, USA) (IF 1:500 and WB 1:1500); mouse anti-myc (Cell Signaling) (IF 1:500 and WB 1:1500).

Secondary antibodies used in this study were: goat anti-rabbit Alexa 555 (Invitrogen, Carlsbad, CA, USA) (IF 1:2000); goat anti-rabbit Alexa 488 (Invitrogen) (IF 1:2000); goat anti guinea pig Alexa 555 (Invitrogen) (IF 1:2000); goat anti guinea pig Alexa 488 (Invitrogen) (IF 1:2000), anti-mouse coupled to HRP (Cell Signalling) (WB 1:10000), anti-rabbit coupled to HRP (Cell Signaling) (WB 1:10000).

Cell surface measurements

The cell surface area of type A intercalated cells (exhibiting basolateral AE1 and apical V-type ATPase B1 subunit localization) was determined in the inner stripe of the outer medulla with ImageJ. Briefly, a grid of arbitrary size was placed on immunohistochemistry pictures and the stained cell area within each grid was calculated as a ratio of unit grid. To avoid biased measurements of type A intercalated cells 5 different randomly selected grid sizes were applied, and the mean was calculated (16). In total, type A intercalated cells from 2 different mice per genotype were measured. Cortical type A intercalated cells were not measured due to weak staining in heterozygous and homozygous Ae1-R607H knock-in mice. The experimenter was blinded for the genotype.

Statistics

The three genotype groups were compared by one-way ANOVA followed by Tukey's multiple comparisons test. P-value < 0.05 was considered significant.

Supplementary Figures

Supplementary Figure 1. (A) Targeting and screening strategy. Top: murine *Ae1* locus; middle: targeted locus; lower: locus after Cre-mediated removal of the selection cassette. (**B**) Clones were screened by Southern blot using *Hind*III and an external probe as indicated. The probe detected a 20 kb wild-type (WT) fragment and a 4.8 kb targeted fragment. (**C**) Histological analysis of mouse kidney sections at 3 months of age revealed no abnormalities (Masson Goldner, scale bar 50 µm). (**D**) Von Kossa stain revealed no detectable nephrocalcinosis (scale bar 50 µm).

Supplementary Figure 2. (**A-G**) After 3 days under standard conditions to determine baseline values, $Ae1^{+/+}$ (n=6; diamond), $Ae1^{+/R607H}$ (n=10; square) and $Ae1^{R607H/R607H}$ (n=8; triangle) mice were acid-challenged for 6 days with 0.28 M NH_4Cl in drinking water. (A) Blood [HCO_3^-]. (B) Blood pCO_2. (C) Urinary net acid excretion (NAE). (D) Urinary titratable acid (TA). (E) Body weight. (F) Water intake. (G) Food intake. Data are presented as mean ± SEM. *P<0.05, **P<0.01, ***P<0.001, ****P<0.0001 as indicated for $Ae1^{+/R607H}$ or $Ae1^{R607H/R607H}$ vs. $Ae1^{+/+}$; other data points not significant; comparison $Ae1^{+/R607H}$ vs. $Ae1^{R607H/R607H}$ revealed no significant difference at any time point (Two-way ANOVA).

Supplementary Figure 3. Grey scaled images of the immunofluorescence stainings displayed in Figure 2. Scale bars: 10 µm.

Supplementary Figure 4. (**A**) Coomassie blue stained gel of RBC lysates from WT (n=4), $Ae1^{+/R607H}$ (n=5), and $Ae1^{R607H/R607H}$ (n=5) mice (**B**) Quantification of Ae1 protein expression normalized to actin. We detected no significant differences between genotypes.

Supplementary Figure 5. Representative western blots for Ae1 protein abundance in protein lysates from cortex (**A**) and medulla (**B**) of WT, $Ae1^{+/R607H}$ and $Ae1^{R607H/R607}$ mice.

Supplementary Figure 6. Representative western blot for pulse-chase experiments. (**A**) M1 cells transfected with human kAE1-WT. (**B**) M1 cells transfected with human kAE1-R589H. (**C**) mIMCD-3 cells transfected with human kAE1-WT. (**D**) mIMCD-3 cells transfected with human kAE1-R589H. Empty circles indicate non-glycosylated protein; filled circles indicate glycosylated protein.

Supplementary Figure 7. Merged channels (**A-C**) for co-immunostainings for the Ae1 (**D-F**) and the B1 subunit of the V-type ATPase (**G-I**) in inner stripe of outer medulla under baseline conditions. Scale bars: 10 µm.

Supplementary Figure 8. Merged channels (**A-C**) for co-immunostainings for the Ae1 (**D-F**) and the B1 subunit of the V-type ATPase (**G-I**) in inner stripe of outer medulla under acid challenge. Scale bars: 10 µm.

Supplementary Figure 9. Immunogold labelling of the A subunit of the V-type ATPase in type B intercalated cells in the cortex. (**A-C**) Overview from WT, *Ae1*$^{+/R607H}$ and *Ae1*$^{R607H/R607H}$ mice. Scale bar: 2 µm. (**D-F**) Higher magnification images of the basolateral cell pole. Scale bar: 1 µm (**G-I**) Higher magnification images of the apical cell pole. Scale bar: 1 µm. (**J**) Pendrin protein abundance analyzed in whole kidney protein lysates is unchanged in *Ae1*$^{+/R607H}$ and *Ae1*$^{R607H/R607}$ mice compared to wild-type mice. Data are presented as means ± SEM; n=5 for wild-type and *Ae1*$^{+/R607H}$, n=4 for *Ae1*$^{R607H/R607H}$ mice.

Supplementary Figure 10. (**A-C**) Renal cortex showing merged channels of the co-staining for Ae1 (red), Pendrin (blue), and the E-subunit (green) of the V-type ATPase. (**D-F**) Single channels for Ae1. (**G-I**) Single channels for the E subunit. (**J-L**) Single channels for Pendrin. Scale bars: 25 µm.

Supplementary Figure 11. (**A-C**) Renal cortex images showing merged channels of the co-staining for Ae1 (red), Pendrin (blue), and Aquaporin 2 (green). (**D-F**) Single channels for Ae1. (**G-I**) Single channels for Aquaporin 2. (**J-L**) Single channels for Pendrin. Scale bars: 25 µm.

Supplementary Figure 12. (**A-C**) Renal cortex images showing merged channels of the co-staining for Ae1 (red), p62 (green), and DAPI (blue). (**D-F**) Single channels for Ae1. (**G-I**) Single channels for p62. (**J-L**) Single channels for DAPI. Scale bars: 25 μm.

Supplementary Figure 13. (**A-C**) Renal medulla images showing merged channels of the co-staining for Ae1 (red), p62 (green), and DAPI (blue). (**D-F**) Single channels for Ae1. (**G-I**) Single channels for p62. (**J-L**) Single channels for DAPI. Scale bars: 25 μm.

Supplementary Figure 14. (**A-C**) Renal cortex images showing merged channels of the co-staining for Ubiquitin (red), p62 (green), and DAPI (blue). (**D-F**) Single channels for Ubiquitin. (**G-I**) Single channels for p62. (**J-L**) Single channels for DAPI. Scale bars: 10 μm.

Supplementary References

1. Schwenk F, Baron U, and Rajewsky K. A cre-transgenic mouse strain for the ubiquitous deletion of loxP-flanked gene segments including deletion in germ cells. *Nucleic Acids Research* 23(24):5080-1, 1995.
2. Hennings JC, Picard N, Huebner AK, Stauber T, Maier H, Brown D, Jentsch TJ, Vargas-Poussou R, Eladari D, and Hubner CA. A mouse model for distal renal tubular acidosis reveals a previously unrecognized role of the V-ATPase a4 subunit in the proximal tubule. *EMBO Molecular Medicine* 4(10):1057-71, 2012.
3. Sinning A, Liebmann L, Kougioumtzes A, Westermann M, Bruehl C, and Hubner CA. Synaptic glutamate release is modulated by the Na^+-driven Cl^-/HCO_3^- exchanger Slc4a8. *The Journal of Neuroscience* 31(20):7300-11, 2011.
4. Cordat E, Kittanakom S, Yenchitsomanus PT, Li J, Du K, Lukacs GL, and Reithmeier RA. Dominant and recessive distal renal tubular acidosis mutations of kidney anion exchanger 1 induce distinct trafficking defects in MDCK cells. *Traffic* 7(2):117-28, 2006.
5. Paunescu TG, Ljubojevic M, Russo LM, Winter C, McLaughlin MM, Wagner CA, Breton S, and Brown D. cAMP stimulates apical V-ATPase accumulation, microvillar elongation, and proton extrusion in kidney collecting duct A-intercalated cells. *American Journal of Physiology* 298(3):F643-54, 2010.
6. Frumence E, Genetet S, Ripoche P, Iolascon A, Andolfo I, Le Van Kim C, Colin Y, Mouro-Chanteloup I, and Lopez C. Rapid Cl^-/HCO_3^- exchange

kinetics of AE1 in HEK293 cells and hereditary stomatocytosis red blood cells. *American Journal of Physiology* 305(6):C654-62, 2013.
7. Sterling D, and Casey JR. Transport activity of AE3 chloride/bicarbonate anion-exchange proteins and their regulation by intracellular pH. *The Biochemical Journal* 344 Pt 1(221-9), 1999.
8. Rust MB, Faulhaber J, Budack MK, Pfeffer C, Maritzen T, Didie M, Beck FX, Boettger T, Schubert R, Ehmke H, et al. Neurogenic mechanisms contribute to hypertension in mice with disruption of the K^+-Cl^- cotransporter KCC3. *Circulation Research* 98(4):549-56, 2006.
9. Kwon TH, Fulton C, Wang W, Kurtz I, Frokiaer J, Aalkjaer C, and Nielsen S. Chronic metabolic acidosis upregulates rat kidney Na^+-HCO_3^- cotransporters NBCn1 and NBC3 but not NBC1. *American Journal of Physiology* 282(2):F341-51, 2002.
10. Maunsbach AB, Vorum H, Kwon TH, Nielsen S, Simonsen B, Choi I, Schmitt BM, Boron WF, and Aalkjaer C. Immunoelectron microscopic localization of the electrogenic Na^+/HCO_3^- cotransporter in rat and ambystoma kidney. *JASN* 11(12):2179-89, 2000.
11. Frische S, Zolotarev AS, Kim YH, Praetorius J, Alper S, Nielsen S, and Wall SM. AE2 isoforms in rat kidney: immunohistochemical localization and regulation in response to chronic NH_4Cl loading. *American Journal of Physiology* 286(6):F1163-70, 2004.
12. Knauf F, Yang CL, Thomson RB, Mentone SA, Giebisch G, and Aronson PS. Identification of a chloride-formate exchanger expressed on the brush border membrane of renal proximal tubule cells. *PNAS* 98(16):9425-30, 2001.
13. Vallet M, Picard N, Loffing-Cueni D, Fysekidis M, Bloch-Faure M, Deschenes G, Breton S, Meneton P, Loffing J, Aronson PS, et al. Pendrin regulation in mouse kidney primarily is chloride-dependent. *JASN* 17(8):2153-63, 2006.
14. Breton S, Wiederhold T, Marshansky V, Nsumu NN, Ramesh V, and Brown D. The B1 subunit of the H^+-ATPase is a PDZ domain-binding protein. Colocalization with NHE-RF in renal B-intercalated cells. *The Journal of Biological Chemistry* 275(24):18219-24, 2000.
15. Stehberger PA, Shmukler BE, Stuart-Tilley AK, Peters LL, Alper SL, and Wagner CA. Distal renal tubular acidosis in mice lacking the AE1 (band3) Cl^-/HCO_3^- exchanger (Slc4a1). *JASN* 18(5):1408-18, 2007.
16. West MJ. Estimating volume in biological structures. *Cold Spring Harbor protocols.* 2012(11):1129-39, 2012.

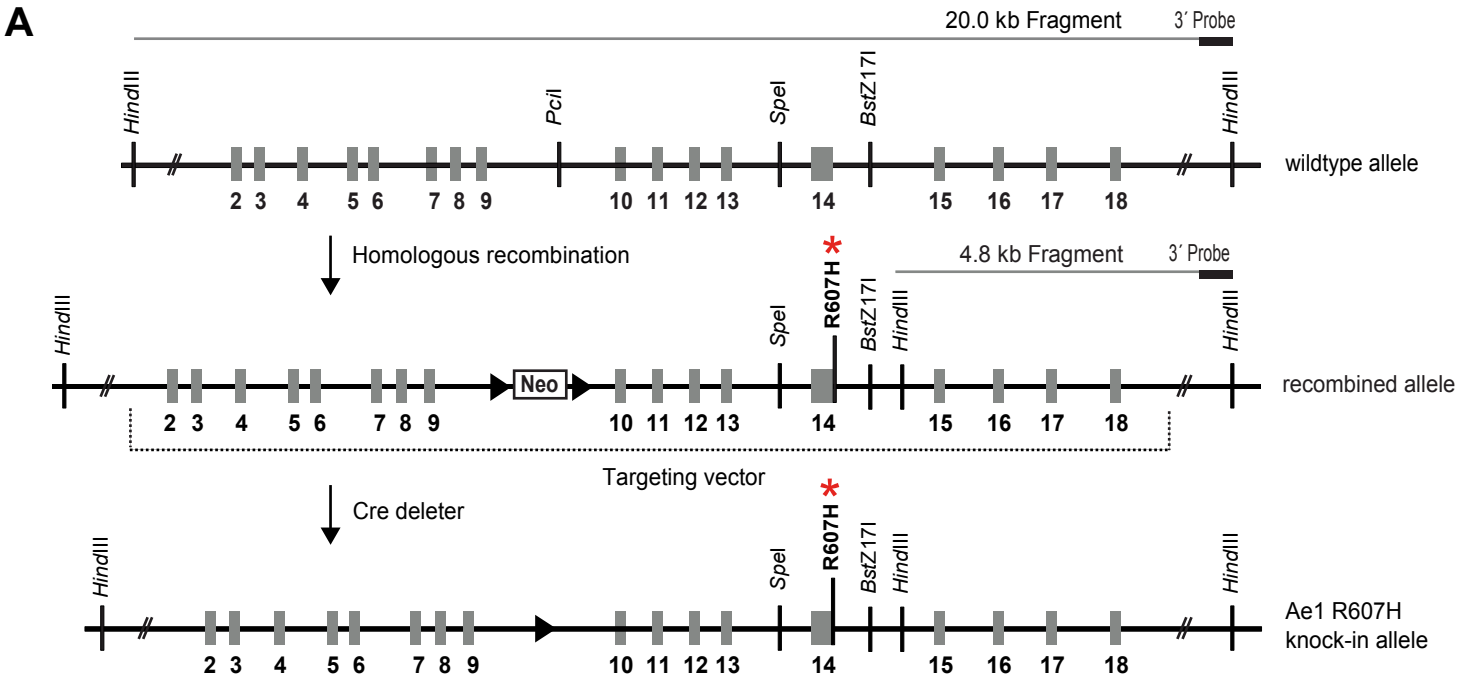

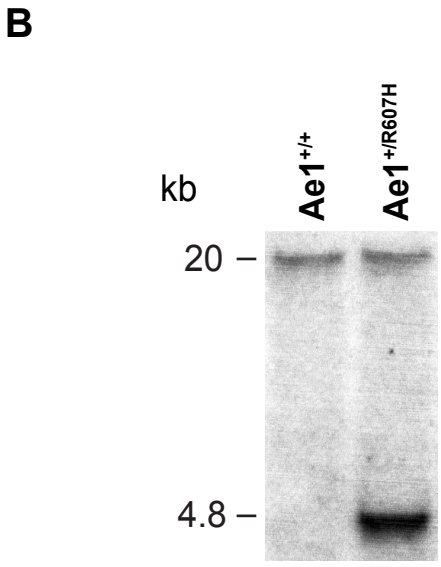

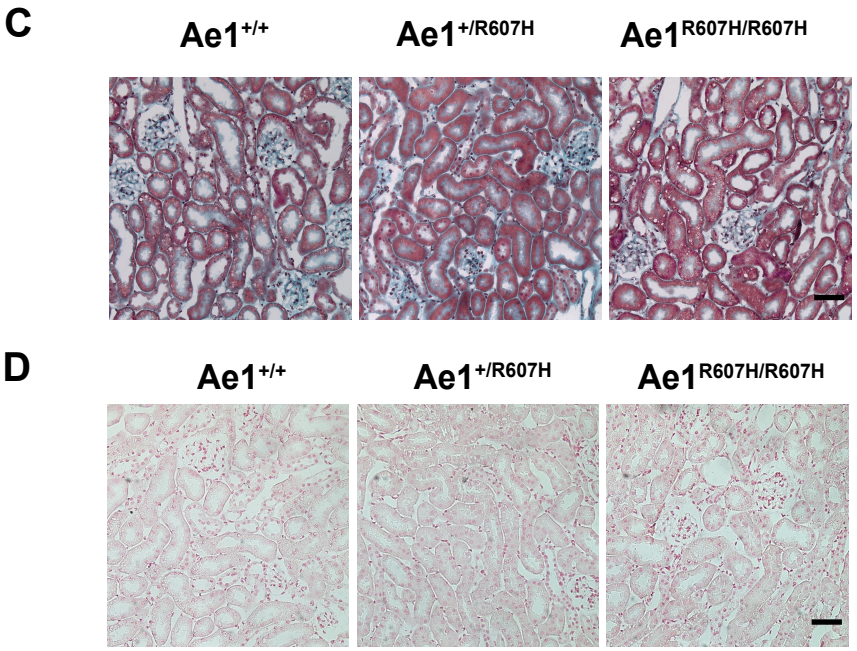

Supplementary Figure: 1

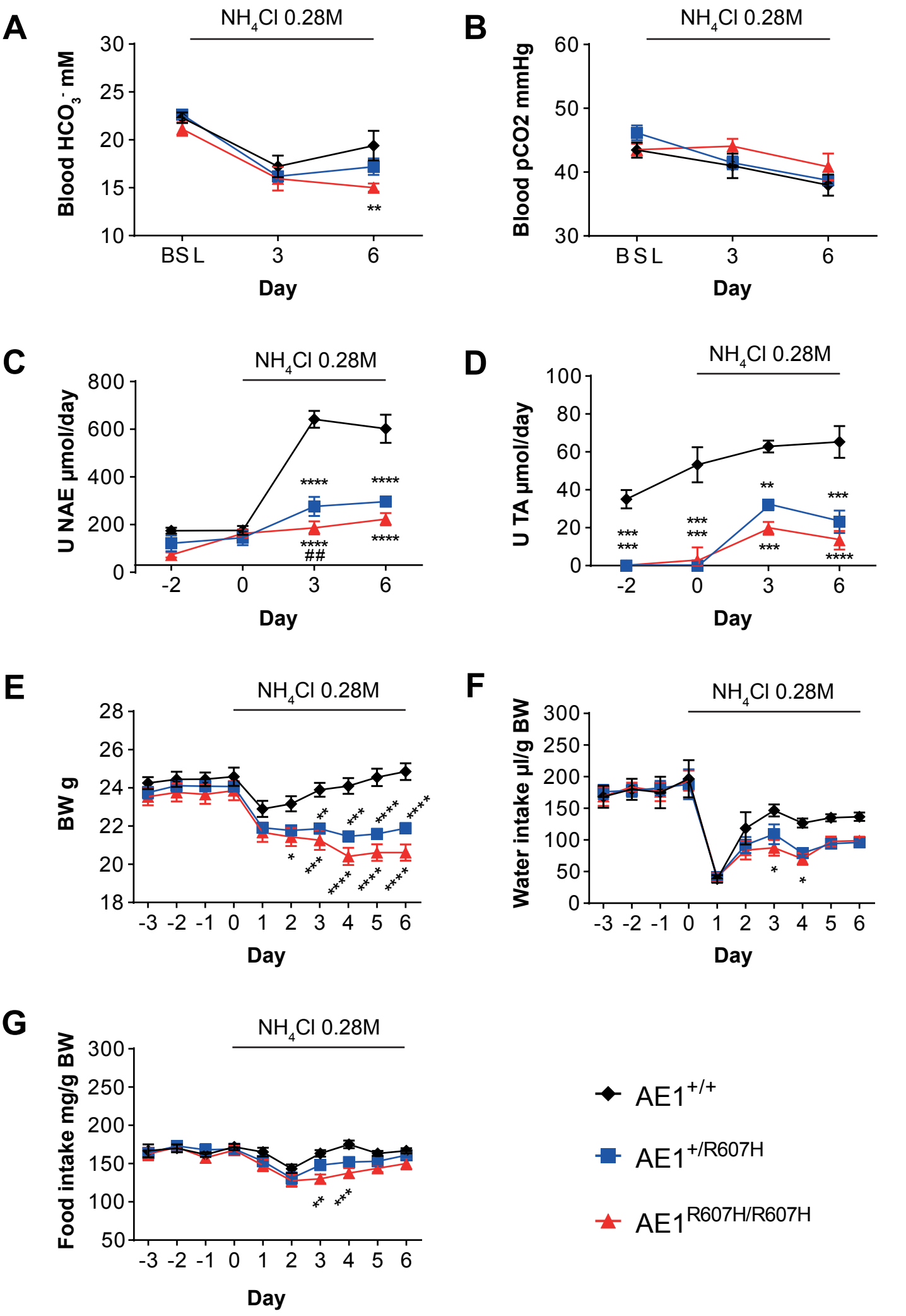

Supplementary Figure: 2

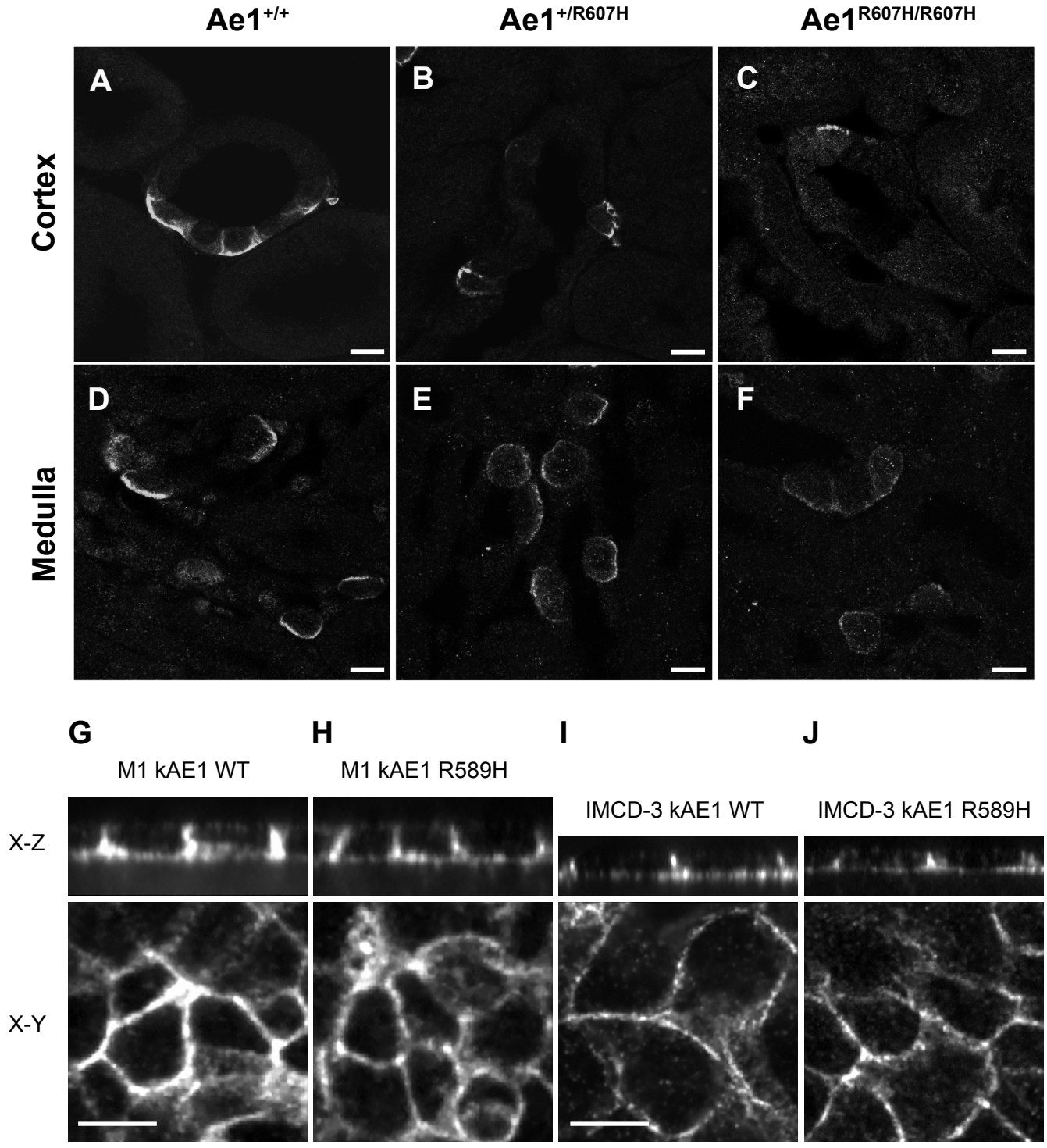

Supplementary Figure: 3

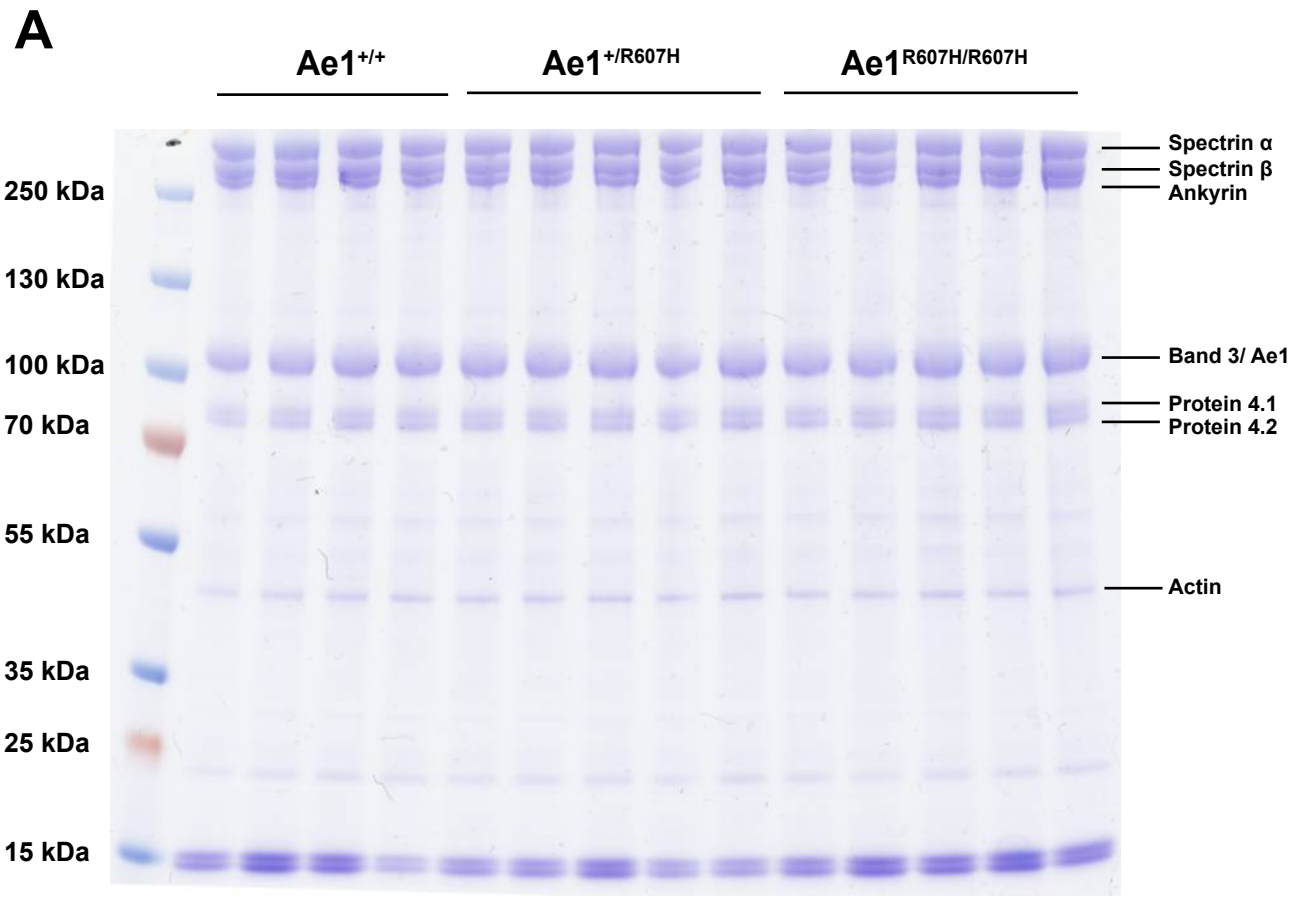

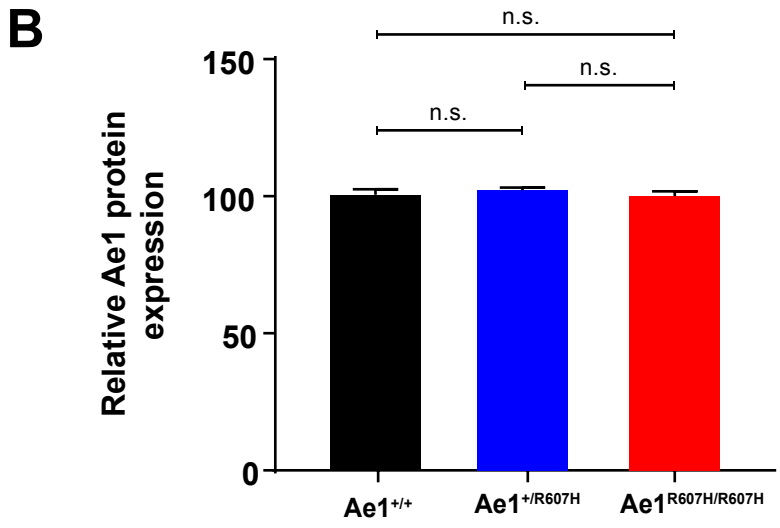

Supplementary Figure: 4

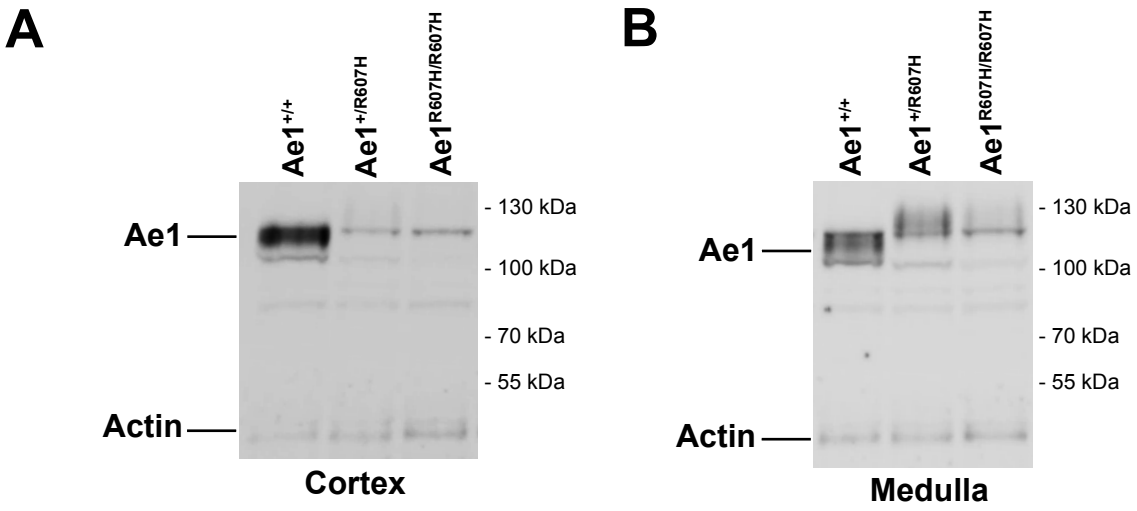

Supplementary Figure: 5

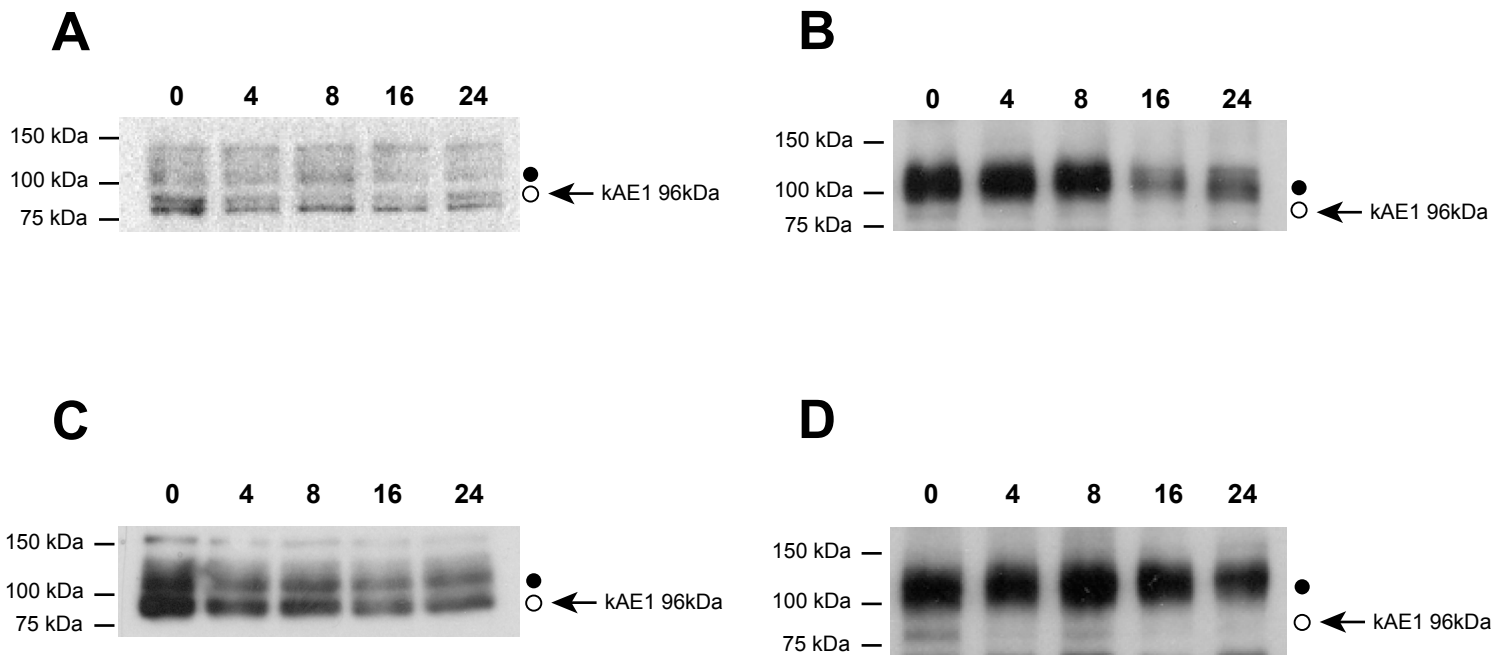

Supplementary Figure: 6

A M1 AE1-WT
B M1 AE1-R589H
C mIMCD3 AE1-WT
D mIMCD3 AE1-R589H

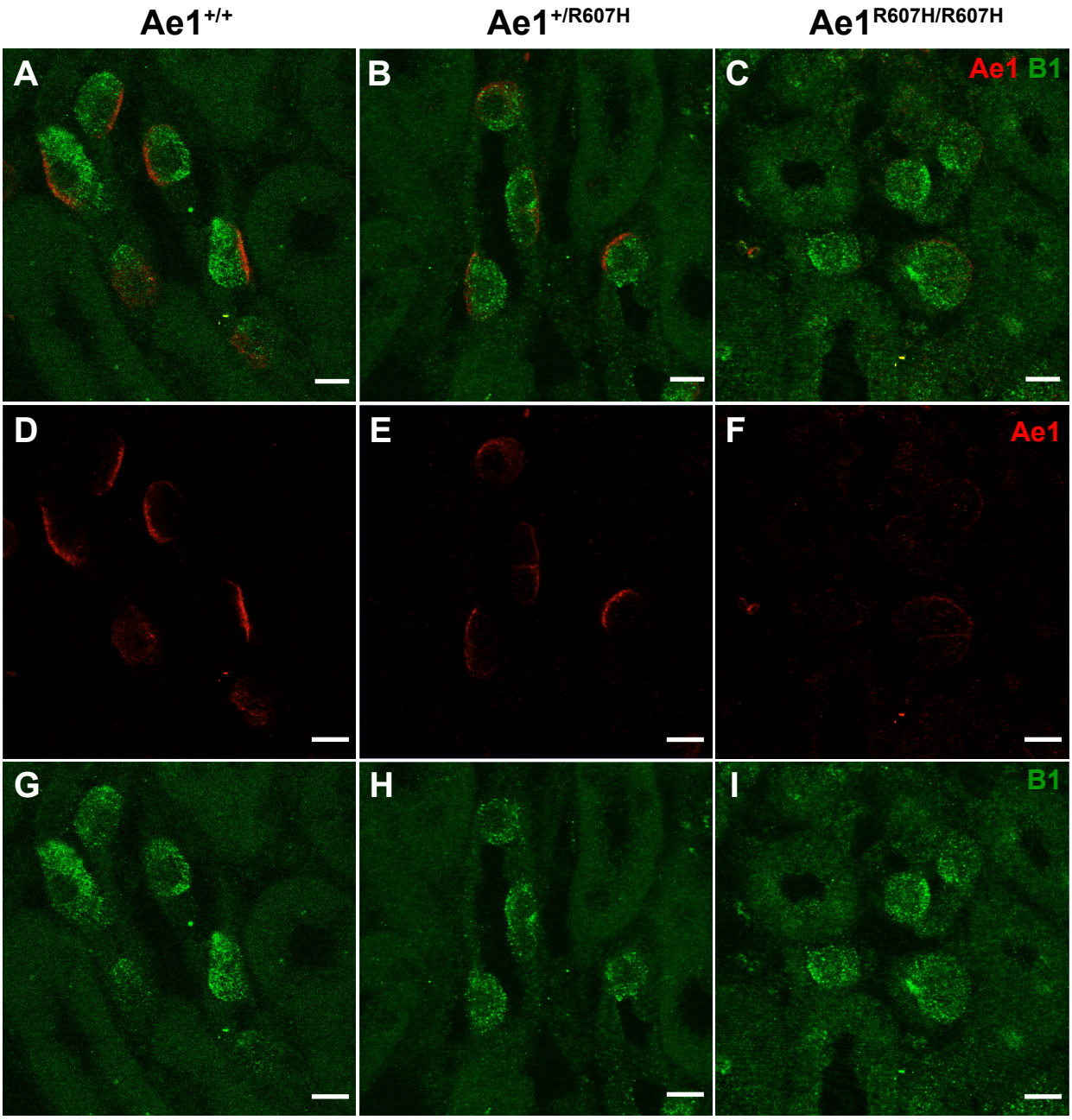

Supplementary Figure: 7

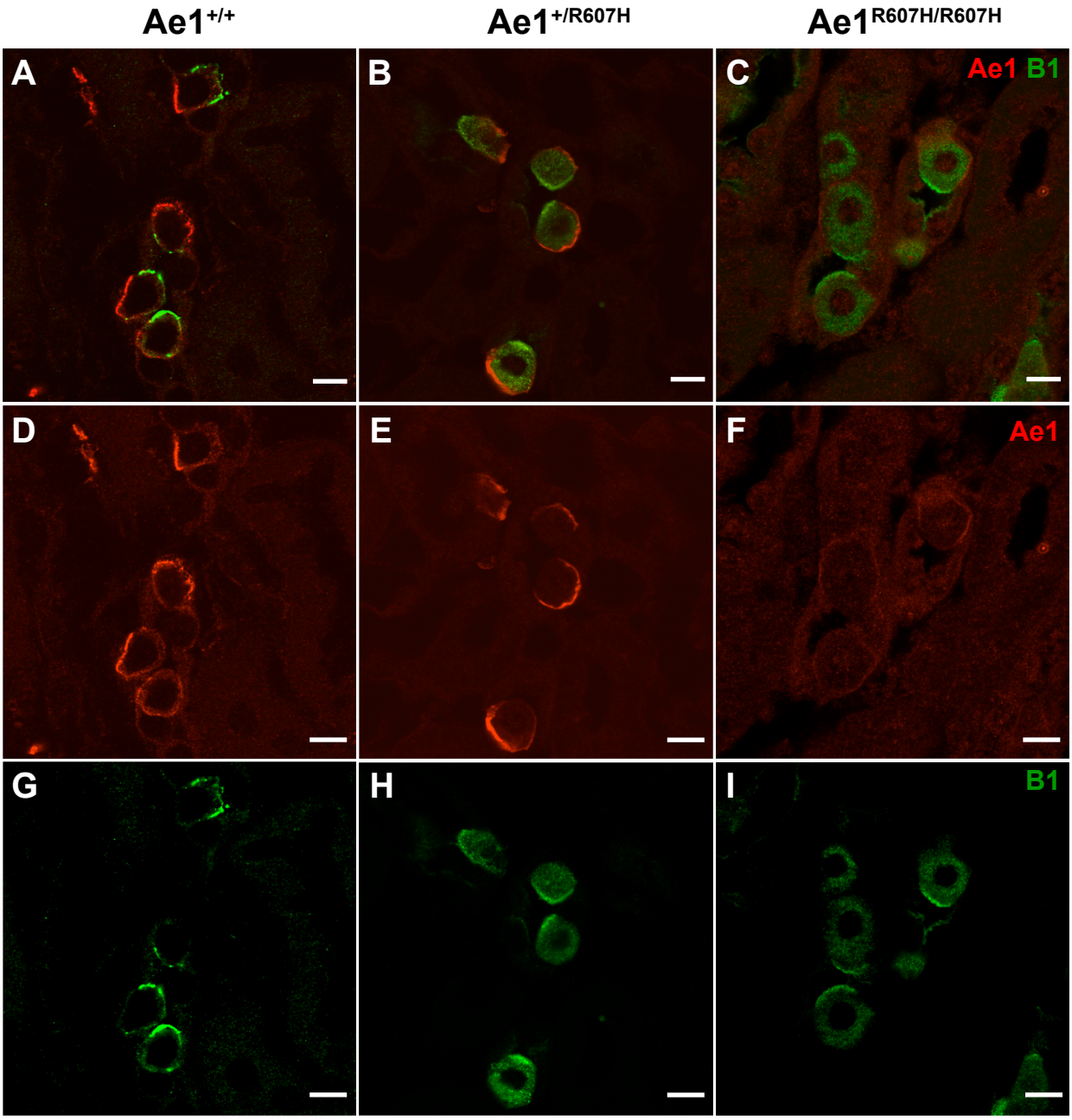

Supplementary Figure: 8

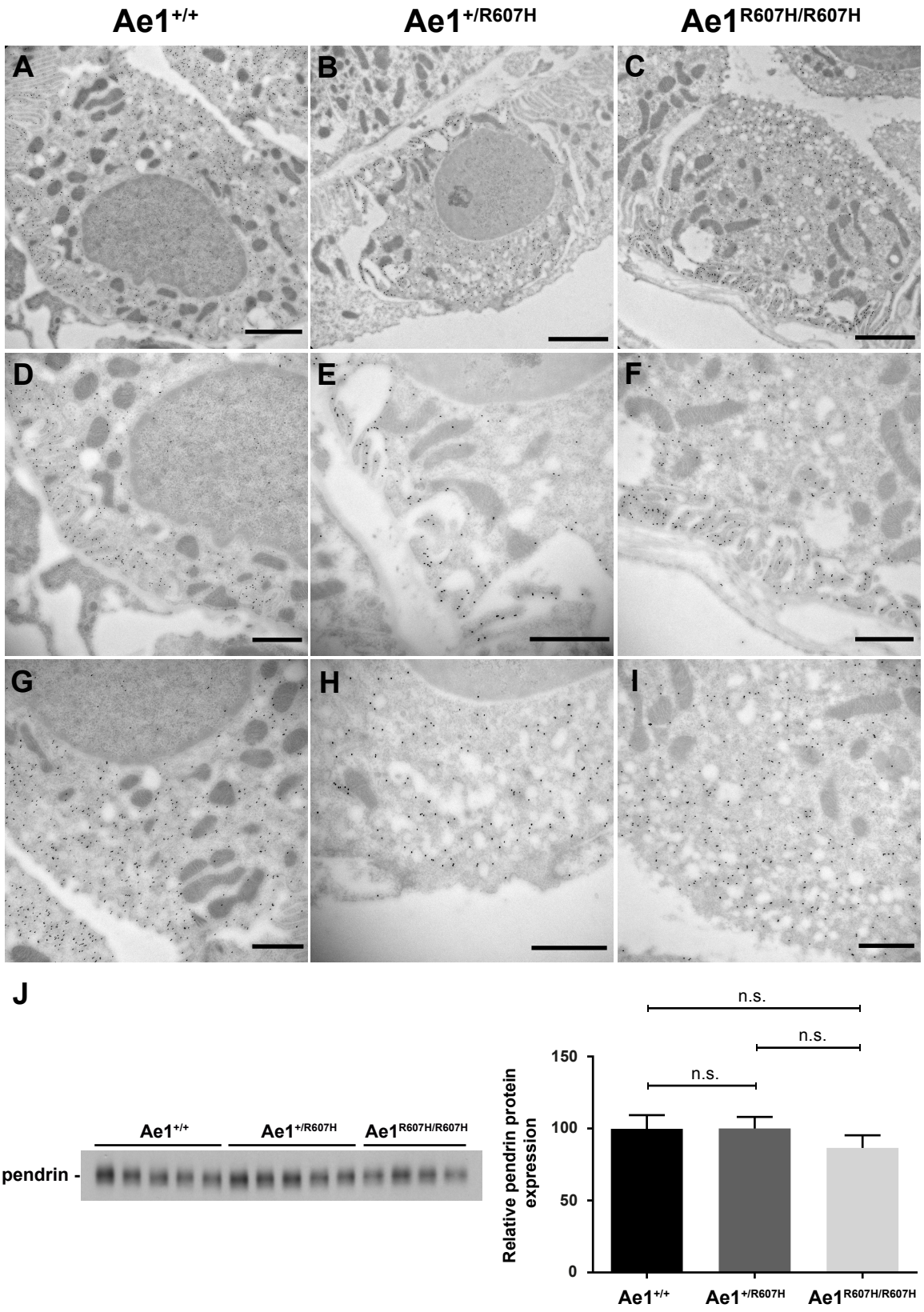

Supplementary Figure: 9

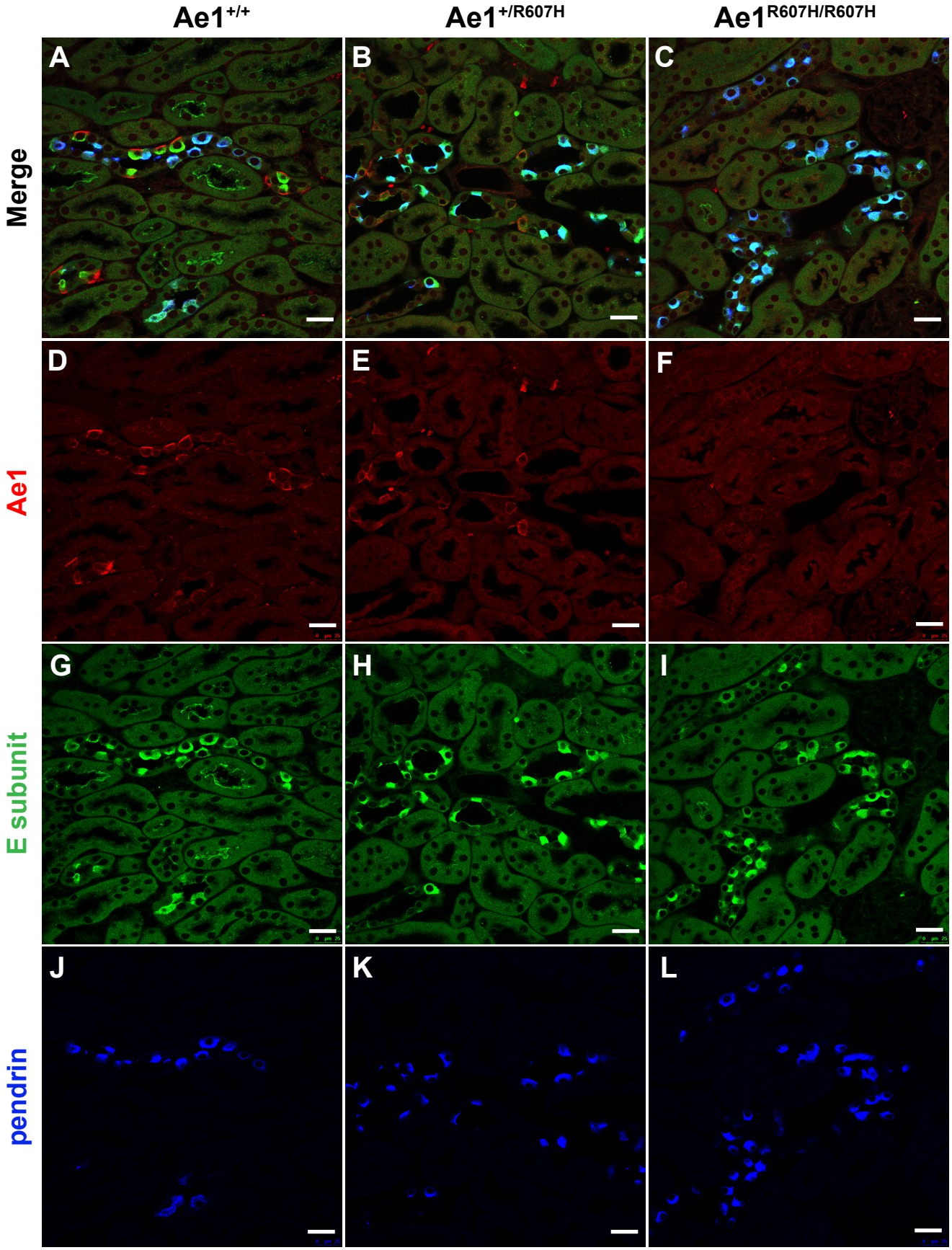

Supplementary Figure: 10

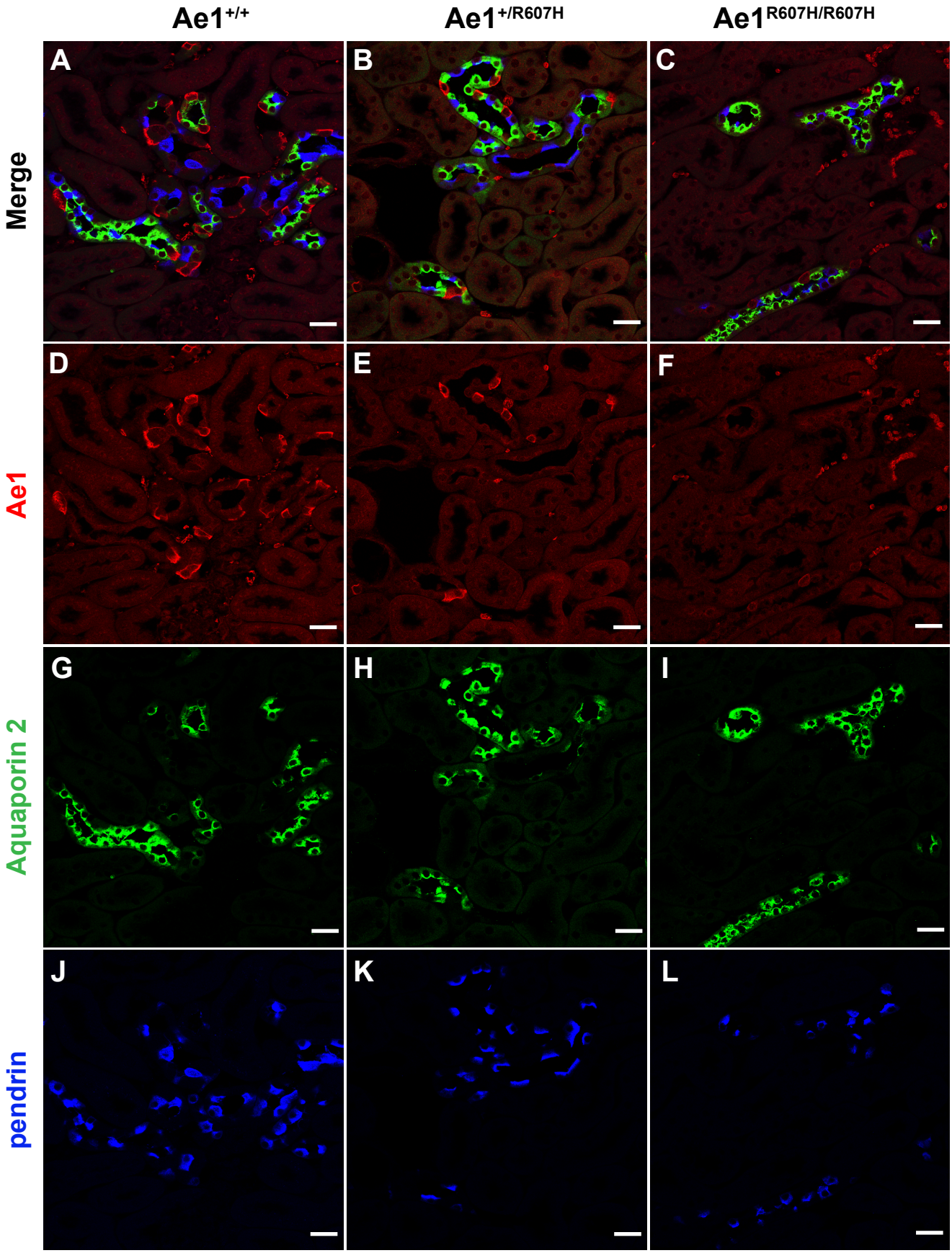

Supplementary Figure: 11

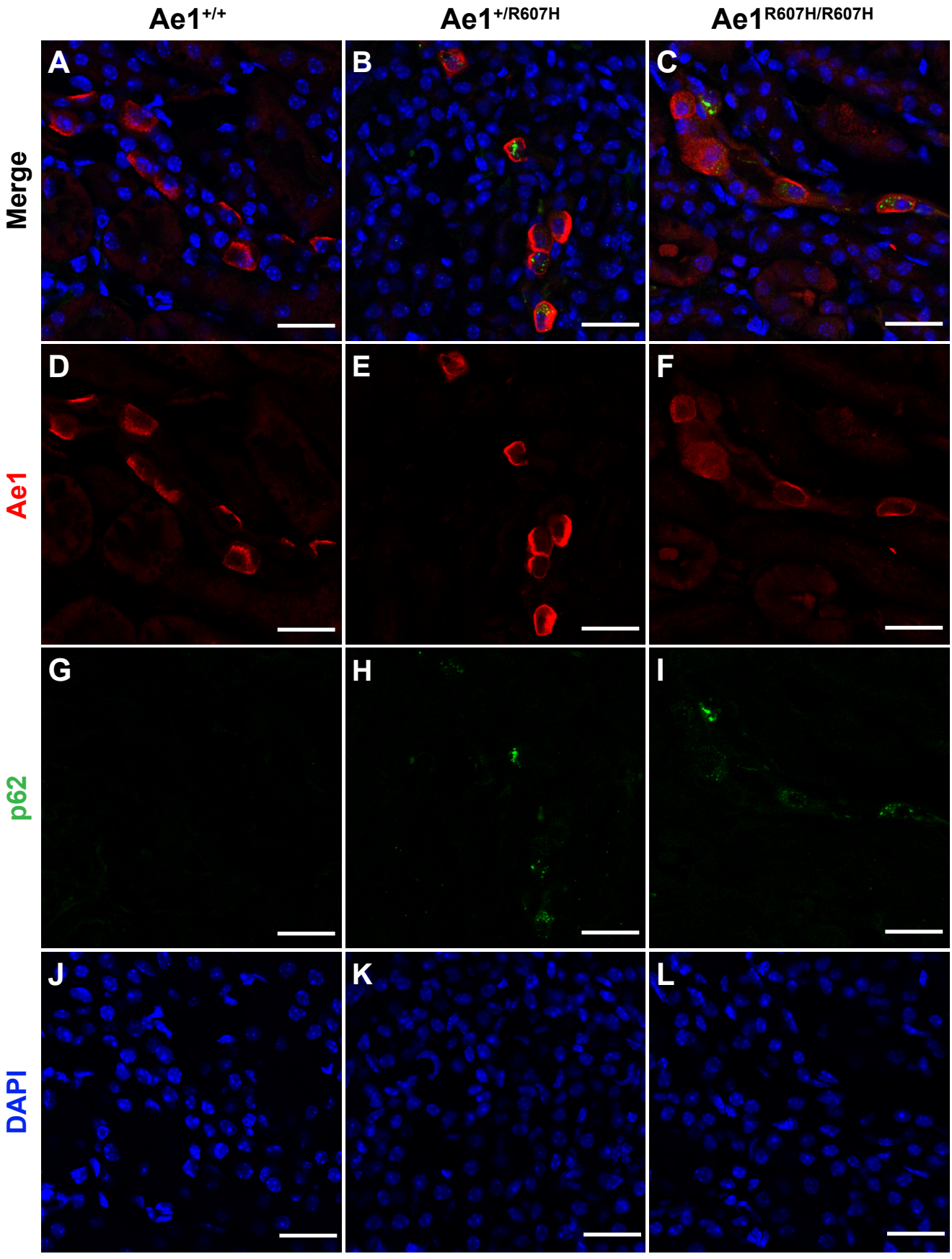

Supplementary Figure: 12

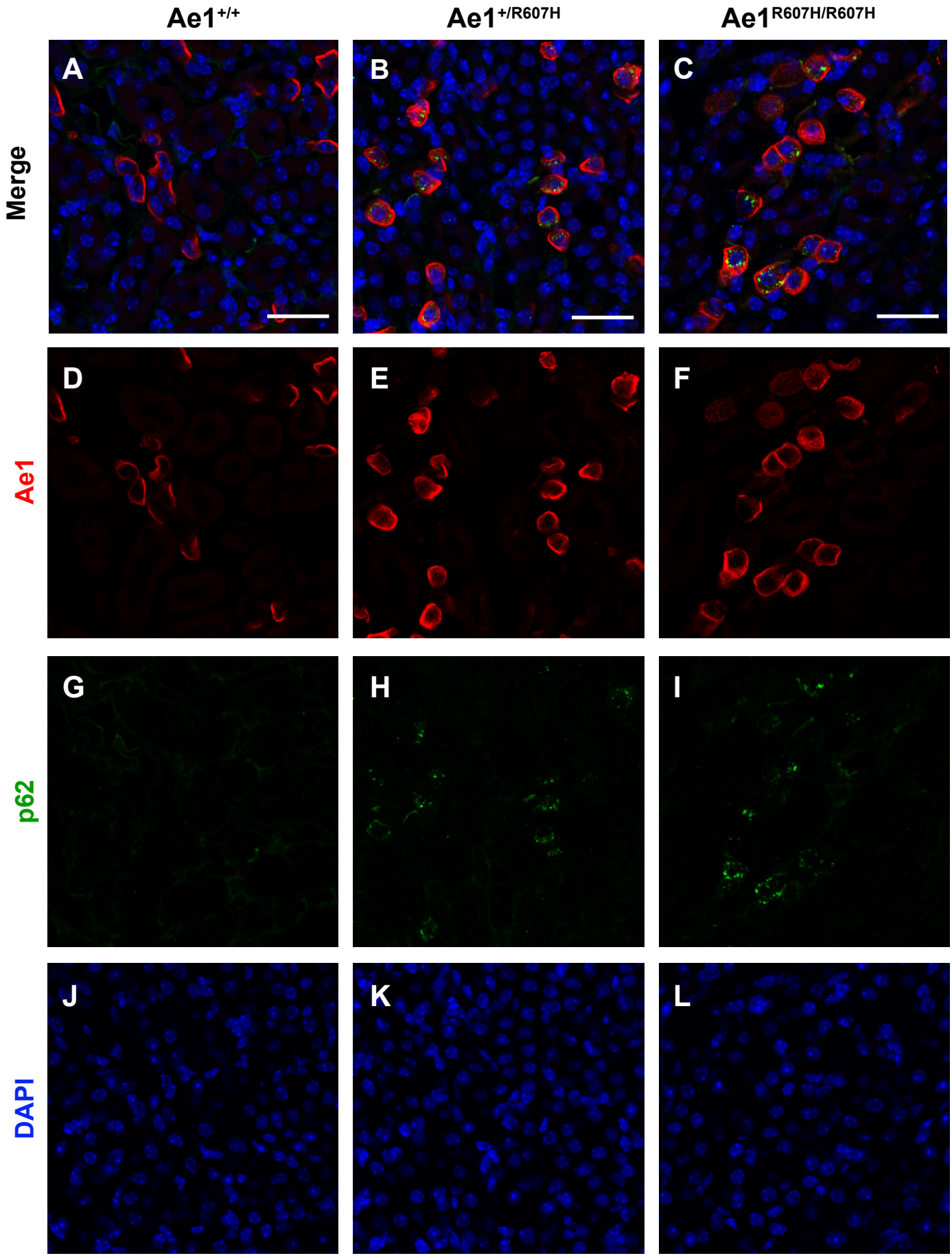

Supplementary Figure: 13

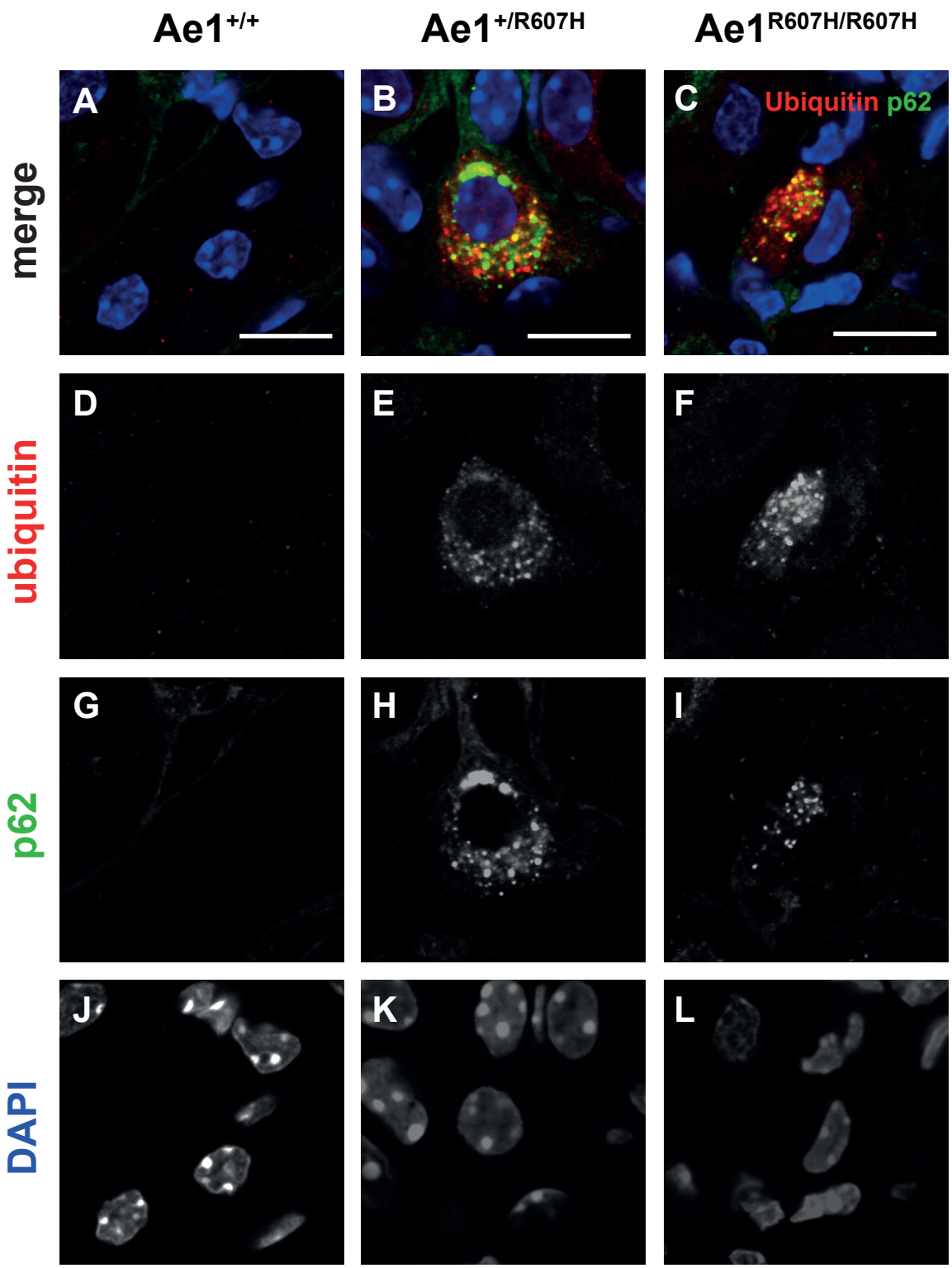

Supplementary Figure: 14